American Mineralogist, Volume 80, pages 715–724, 1995

Mica polytypism: Identification and origin

Hiroshi Takeda
Mineralogical Institute, Faculty of Science, University of Tokyo, Hongo, Tokyo 113, Japan
Malcolm Ross
U.S. Geological Survey, National Center 959, Reston, Virginia 22092, U.S.A.

Abstract

Practical methods for identification of the complex mica polytypes have been developed by introducing a special function characteristic of their layer stacking sequences that is displayed in their X-ray diffraction patterns. This periodic intensity distribution (PID) function is the Fourier transform of a stacking sequence. The X-ray diffraction patterns of a polytype are expressed by the PID function modified by the Fourier transform of the unit mica layer. The PID function is used to determine the stacking sequences of several polytypes, and the mechanism by which the most frequently observed polytypes form is discussed. The axial settings of mica polytypes are defined in order to compute the PID functions in terms of the layer stacking sequences. Practical methods of obtaining observed PID functions are given together with tables of the PID functions of the three basic polytype series. The common polytypes have the basic sequences such as $1M$, $3T$, and $2M_1$ and are modified by a stacking fault, but the subsequent sequences are so arranged that the original direction of stacking is recovered as readily as possible.

Introduction

Until 1966 only the layer stacking sequences of the $1M$, $2M_1$, $2M_2$, and $3T$ mica polytypes (Smith and Yoder, 1956) were known. The systematic derivation of mica polytypes and their X-ray diffraction patterns (Takeda, 1967) enabled us to describe the layer stacking sequences of more than ten complex mica polytypes having unit cell dimensions from 40 Å to more than 200 Å in the **c*** stacking direction (Ross et al., 1966). Subsequent X-ray and electron diffraction analysis and transmission electron microscopy investigations (for example, Rieder, 1970; Pandey et al., 1982; Rule et al., 1987; Baronnet and Kang, 1989) have shown that mica polytypes possess some of the most complex inorganic structures known.

One of the difficulties in determining the layer stacking sequence of micas by X-ray diffraction techniques is the relatively large size of the unit layer in comparison with that of silicon carbide. A characteristic feature of X-ray diffraction patterns of mica polytypes is a periodicity of the intensity distribution along reciprocal lattice rows parallel to **c*** of the crystal. However, such periodicity can be more easily recognized after elimination of the modulation by the Fourier transform of the complex unit layer. In general, the periodicity is observed when the crystal structure involves only displacements of identical unit layers. The outline of preliminary theory and an example of its application for this periodic intensity distribution (PID) function is given in a previous manuscript (Takeda, 1967).

Another difficulty is the frequent presence of twinning. Those apparent polytypes that have unit cell repeats in multiples of three have often been mistaken as complex mica polytypes. An analysis of simple $1M$ and $2M_1$ twinning has been developed by Sadanaga and Takéuchi (1961). More complex twinning, consisting of more than three individuals of one kind of polytype or the coalescence of two or more kinds of polytypes, has been discussed by Rieder (1970). A thorough twin analysis should be completed before the application of the PID function.

General representations of polytypism are given in the IUCr report (Guinier et al., 1984), and applications of the OD-theory are mentioned by Dornberger-Schiff et al. (1982) and Weiss and Wiewiora (1986). To represent the stacking sequences of mica polytypes, three different symbolisms have been proposed (Zvyagin, 1960; Ross et al., 1966; Takeda and Sadanaga, 1969). A method of deriving the space groups in terms of one of these symbolisms, together with a method of generating all possible stacking sequences for a given layer number, was given previously by Takeda (1971). To derive the PID function, the symbols representing interlayer rotations must be transformed to symbols that give layer positions for a particular set of crystallographic axes. A procedure to calculate the PID functions is given here and is compared with observed PID values of polytypes frequently found in nature. Because the number of possible polytypes increases very rapidly for micas with larger layer repeats, a major limitation of the application of this method rests on the availability of fast computers (Mogami et al., 1978).

The three basic series of complex mica polytypes were discovered through the application of the PID function

0003–004X/95/0708–0715$02.00

Table 1. Atomic coordinates in the hexagonal setting of a mica unit layer with symmetry $1P\bar{3}1m$

Atoms	x	y	z
$\frac{1}{2}M_o$	0	$\frac{1}{3}$	$\frac{1}{2}$
OH	0	0	$\frac{1}{2} - t_o$
O_a(apical)	$\frac{2}{3}$	$\frac{1}{3}$	$\frac{1}{2} - t_o$
M_i	$\frac{2}{3}$	$\frac{1}{3}$	$\frac{1}{2} - t_o - d_i c^*$
O_b(basal)	$\frac{1}{2} + \sqrt{3}/6\tan\alpha$	0	$\frac{1}{2} - t_o - \frac{1}{3}d_i c^*$
K	0	0	0

Note: $\tan\alpha = 4\sqrt{2}\cdot\sqrt{(d_i/b)^2 - \frac{1}{32}}$, $c^* = 1/(c\sin\beta)$, $d_o\cos\psi = b\sqrt{(d_o/b)^2 - \frac{1}{27}}$, $t_o = d_o\cos\psi c^*$.

Table 2. Components of displacement vectors in the orthogonal coordinate for the six stacking operators

Rotation around **c*** (°)	Stacking operators (r)	Elements of stacking operators† (x_r, y_r)
0	0	−1, 0
60	1	1, 1
120	2	−1, 1
180	3	1, 0
240	4(−2)	−1, −1
300	5(−1)	1, −1

† The elements are expressed in the unit of $\frac{1}{3}a$, $\frac{1}{3}b$.

(Ross et al., 1966); this work demonstrated that the polytypism of micas resembles that found in the silicon carbide polytypic series. This resemblance suggests that theories of polytype formation proposed silicon carbide may also be applied to micas. Baronnet (1975) showed a relationship between growth spirals and the formation of complex mica polytypes. Application of the faulted matrix model to the growth of mica polytypes was undertaken by Baronnet et al. (1981) and Pandey et al. (1982). Baronnet and Kang (1989) reviewed the crystal growth aspects of mica polytypism with emphasis on the relationships between the growth mechanisms of the basal faces and ordering of the unit modules within the mica structure.

Models of the mica unit layer

The conventional unit layer that is used to derive mica polytypes is one layer of the $1M$ monoclinic mica (Smith and Yoder, 1956). The symmetry of this layer is best described by one of the 80 layer-group symbols (diperiodic group or two-translational three-dimensional group, $1C2/m$ after Niggli, personal communication) (Wood, 1964). Even though the refinements of the $2M_1$ (Burnham and Radoslovich, 1964) and $3T$ (Güven and Burnham, 1967) moscovite and other structures in subgroup symmetries have shown that the true symmetry of the unit layer is lower than $1C2/m$, this idealized $1C2/m$ is realized to a very good approximation in all mica polytypes for the purpose of deriving their Fourier transforms.

To describe a mica polytype without rotations of the unit layers, Sadanaga and Takeda (1968) and Takeda and Sadanaga (1969) chose a layer designated as the TS unit layer, which is composed of a plane of alkali ions in the center and octahedral cations on both sides (see Fig. 1 of Takeda and Sadanaga, 1969). The choice of the TS unit layer explains the symmetry of diffraction patterns of micas better than the conventional unit layer. It is recognized that the layer-group symmetry is $1P\bar{3}1m$, which is higher symmetry than $1C2/m$. This layer, as described above, having layer-group symmetry $1P\bar{3}1m$, is designated the D layer (ditrigonal layer). A model of the D layer can be predicted from the unit cell dimensions and cation-to-O distances (Table 1) within tetrahedral and octahedral sheets (Takeda and Morosin, 1975).

The D layer of the TS unit layer model given by Takeda and Sadanaga (1969) is applicable only to polytypes with 0, 120, or 240° rotations. To describe all other polytypes, we introduce additional unit layers, in which a 60, 180, or 300° rotation of the atoms in the lower half of the unit cell forms a trigonal prism around the alkali cation (K or Na). The layer-group symmetry of this type of TS unit layer is $mP32m$ (see Fig. 3 of Takeda and Sadanaga, 1969) and is designated as a T layer (trigonal layer). A 180° rotation of the T layer about the axis perpendicular to the layer was designated as the T* layer. The same 180° rotation of the D layer gives the D* layer.

Using these four unit layers (D, D*, T, and T*), Takeda and Sadanaga (1969) showed that all the stacking sequences of the mica polytypes could be expressed with only the displacements of these layers along the $\pm\mathbf{a}$ and $\pm(\mathbf{a} + \mathbf{b})$ axes of the hexagonal cell (perpendicular to the **c** axis and without any rotational operations). The components of displacement vectors in orthogonal coordinates for the six stacking operations are listed in Table 2. For the polytypes with only the D layers involving 0, 120, and 240° rotations and with $1M$-type axial setting, the shifts of layers are only along the **a** axis, and the amount of shift with respect to the preceding one is always $-\frac{1}{3}a$. However, the axial settings for general polytypes must be chosen in accordance with their total displacements as explained below.

Symbols of mica polytype stacking sequences

Amelinckx and Dekeyser (1953) were the first to use a symbol and a diagram to illustrate a mica polytype structure. Their diagram, employed also by Smith and Yoder (1956), is an elegant graphical model of describing the stacking sequences by utilizing the interlayer cation-cation vectors in the mica structure projected on (001). Amelinckx and Dekeyser's numerical representation of stacking sequence are the same as that used later by Zvyagin (1960), who used the alphabetic designations A, B, and C instead of the numbers 1, 2, and 3 to express the orientation of a layer relative to the standard coordinates.

The Zvyagin oriented stacking symbol (Z symbol) expresses the stacking sequence of the N-layer mica with a series of N letters, the jth letter of the series referring to the absolute orientation of the jth layer. By this symbol, the same stacking sequence may be expressed in several ways depending on how one defines the standard axes.

The vector stacking symbols (RTW symbol) of Ross et al. (1966) give the relative rotations between adjacent layers, and they do not depend on the axial setting. Within the brackets of the RTW symbols are N numbers, where N is the number of mica layers per unit cell. The jth number (A_j) of the stacking symbol, where j designates any particular number in the sequence of N numbers, refers to the relative angle of rotation between the jth and $(j + 1)$th mica layer. The letter A_j can have the values 0, ± 1, ± 2, or 3 that refer, respectively, to 0, ± 60, ± 120, and 180° relative rotations of the adjacent layers.

Even though the RTW symbols are useful in generating all the possible mica polytypes with a given layer repeat, the Z symbols are much more convenient in deriving the intensity distribution functions of micas (Takeda, 1967). However, even the Z symbols give only the orientations of the layers and not the positions of the layer in the standard coordinates. The positions must be derived indirectly with the aid of the RTW or Z symbols.

By using the model of a mica unit layer proposed by Takeda and Sadanaga (1969), it is possible to derive symbols that give the positions of the individual unit layers of the stacking sequence (TS symbol); the stacking of layers in this case involves only the displacements of the unit layers. A direct derivation of the TS symbols facilitates the calculation of the PID functions. The TS symbols give the position of the layer in the specified axial setting, together with the type of the unit layer. Polytypes with 0, 120, and 240° rotations and with the 1M-type axial setting are the ones most frequently found in nature.

Since these symbols are composed of a string of numbers consisting of 0, 1, or 2, they can be regarded as ternary numbers. By convention, we express the sequence by the string that gives the minimum decimal number. These abbreviated symbols are useful both in generating all possible polytypes with a given layer number and in computing PID functions. The symbol can be generated directly by applying the principles used in enumerating RTW symbols, and the derived symbol itself expresses the positional coordinates in the particular axial setting.

To convert the RTW symbol into the TS symbol, use is made of a stacking operator, which causes displacement of the unit layer, in accordance with the interlayer rotation as expressed by each element of the symbol. This operation is performed in an orthogonal C-centered crystal structure, and the resulting symbol is transformed into the final symbol in accordance with the proper axial setting of each polytype (Takeda and Sadanaga, 1969). The jth operator r_j in the sequence is expressed as $r_j = \mathrm{mod}(\omega_{j-1} + A_j, 6)$ where ω_{j-1} is a number indicating the orientation of the layer, for which the operator is to be applied (in the same way of expressing the rotation angles as that used in the RTW symbols), ω_{j-1} is equal to r_{j-1} except for ω_0, A_j is the RTW symbol of the jth conventional layer, and mod indicates the mod function. This function mod(n, 6) expresses a number n, in the form of m mod 6, where m is an integer from 0 to 5.

The stacking symbol of the jth layer, s_j or (X_j, Y_j), can be obtained from that of the $(j - 1)$th using the jth operator r_j as $s_j = s_{j-1} \cdot r_j$ or $(X_j, Y_j) = (X_{j-1}, Y_{j-1}) \cdot (x_{rj}, y_{rj}) = (X_{j-1} + x_{rj}, Y_{j-1} + y_{rj})$. For the first layer, s_0 must be set to $(X_0 = 0, Y_0 = 0)$. The elements of the six stacking operators x_{rj} and y_{rj} are given for each r in Table 2.

As was mentioned before, the RTW symbols do not depend on axial orientation, whereas the TS symbols depend on the axial setting. Therefore, the symbols obtained by applying the stacking operators in succession are not always compatible with the orthorhombic or monoclinic settings that so conveniently describe the polytype structures. To be consistent with one of these axial settings, the last symbol, (X_N, Y_N), which expresses components of the total displacements, must have at least one zero element. That is, (X_N, Y_N) must be in the form $(-1, 0)$, $(0, -1)$, or $(0, 0)$ depending upon their respective axial setting (Takeda and Sadanaga, 1969). The orientation of the polytypes is set by the initial values of ω, namely, ω_0. If the last symbol has no zero element, the same process of converting the symbols must be repeated by changing the value of ω_0.

For those polytypes with the axial settings other than orthogonal, the following transformation from the orthogonal setting to the monoclinic one must be applied: For $(-1, 0)$-type, $X_j = X'_j + Z'_j$ and $Y_j = Y'_j$, and for $(0, -1)$-type, $X_j = X'_j$ and $Y_j = Y'_j + Z'_j$, where X'_j, Y'_j, and Z'_j are the elements of the jth stacking symbol in the old orthogonal setting.

The inverse conversion, namely from the abbreviated TS symbols to the RTW symbols, is also important. This conversion can be accomplished with simple algorithms. An intermediate symbol, the binary-represented symbol B_j of the RTW symbol A_j of the jth layer, is expressed in terms of the new symbols Y_j, Y_{j+1}, and Y_{j+2} of the jth, $(j + 1)$th, and $(j + 2)$th layer as

$$B_j = \mathrm{mod}(Y_j + Y_{j+1} + Y_{j+2}, 3) \qquad (1)$$

where mod(m, 3) is the mod function as explained before.

In Equation 1, when $j + 1$ or $j + 2$ (or both) have values greater than N, the total layer number, the symbol Y of the $(j + 1 - N)$th or $(j + 2 - N)$th must be used. To convert the binary-represented symbols into the normal RTW symbols, one must replace the number 2 by -2, and 1 by 2, and leave the 0 symbol as it is.

These transformation routines have been included in the program PTIDN written in FORTRAN IV (this program is available from the senior author upon request), which generates all the possible stacking symbols and computes the intensity distribution functions. A more detailed explanation of the RTW symbols and the TS symbols is given by Takeda and Sadanaga (1969).

Fourier transforms of the unit layers and the PID function

To study the nature of the Fourier transform of complex mica polytypes, the Fourier transforms of the unit layers of the four different layer types must be analyzed, especially with reference to their symmetry relation in

reciprocal space. The same PID function can be derived more simply by the introduction of an unconventional unit layer of mica (Sadanaga and Takeda, 1968). With the aid of this model unit layer, the derivation of the PID function can be treated as involving only displacements of unit layers, and all four Fourier transforms for the D, D*, T, and T* layers have identical values for the following reflections along the c^* reciprocal lattice rows:

$$\begin{aligned} hk^*l \text{ with } h &= 0 \bmod 3, \quad k \text{ no condition;} \\ \text{with } h &= 1 \bmod 3, \quad k = 0 \text{ or } 2 \bmod 3; \\ \text{with } h &= 2 \bmod 3, \quad k = 0 \text{ or } 1 \bmod 3 \end{aligned} \tag{2}$$

where hk^*l is the Miller index (diffraction symbol) for the hexagonal axes. An example of the Fourier transform of a representative mica unit layer is given in Figure 2 of Takeda (1967). These indices should be transformed to the hexagonal reciprocal lattice row $10l$ when the computation is based on the parameters given in Table 1.

In general, the Fourier transform of an N-layer mica polytype is given as (Takeda, 1967)

$$G^N(hkl) = \sum_{j=1}^{N} G_j(h'k'l')\exp 2\pi i[h\Delta x_j + k\Delta y_j + l(j-1)] \tag{3}$$

where $G_j(h'k'l')$ is the Fourier transform of the jth unit layer with indices transformed in accordance with its interlayer rotation around **c***, and Δx_j, Δy_j, and $(j-1)$ are the components of a displacement vector from the origin to the jth layer, along the axes **a**, **b**, **c**, respectively. Because of the symmetry inherent in the Fourier transform of the unit layer, $G_j(h'k'l')$ can be replaced by the Fourier transform of the unit layer before the transformation, $G_0(hkl)$. Thus, the intensity distribution is given by the product of $G_0(hkl)$ and the sum of the exponential terms, S^N. The S^N terms are designated as the PID (periodic intensity distribution) function: $|G^N| = |G_0| \times |S^N|$.

The PID function is a special type of fringe function (Lipson and Taylor, 1958); its value squared and divided by N (for the N-layer mica) has a form of the interference function (Guinier, 1963), where the unit scattering power is divided by the square of the structure factor of the group of atoms under consideration. However, the interference function is in general not a periodic or discrete function, which is characteristic of the S^N function. A set of N values of the S^N function is characteristic of the layer stacking sequence of polytypes and has been used effectively in the determination of the stacking sequence by systematically generating S^N values for all possible N-layer polytypes. A computer program (PTST) has been written to compute the PID function from the RTW symbol (the program is available from senior author upon request).

In the above discussion, we assume that the Fourier transforms of the D, D*, T, and T* layers are exactly identical at those reciprocal lattice nodes given in Equation 2. If there are deviations from the ideal model, weak reflections that violate the structural extinction rules and slight deviation of the periodicity will be observed.

Experimental procedure to obtain the PID function

To characterize the mica polytype by X-ray precession photography most easily, the following procedure was used. The mica plate was mounted so that the (001) plane was perpendicular to the goniometer rotation axis of the precession camera. Adjustment of the goniometer arcs was made so that **c*** was coincident with the dial axis. Rotation of the crystal about the dial axis was made until a principal reciprocal lattice net was found. This was either the $h0l$, $h3hl$, $\bar{h}3hl$, $0kl$, hhl, or $\bar{h}hl$ net for any mica polytype. The $h3hl$ and $\bar{h}3hl$ nets are $\pm 60°$ from the $h0l$ position, the hhl and $\bar{h}hl$ nets are $\pm 60°$ from the $0kl$ position, and the $0kl$ net is 90° from the $h0l$ position. For many polytypes, the $0kl$ net is orthogonal. For trioctahedral micas, it is generally not possible to differentiate the $h0l$, $h3hl$, and $\bar{h}3hl$ nets from one another by casual inspection because of the pseudotrigonal nature of the mica structure.

Using six single-crystal diffraction photographs of the above mentioned nets, any mica polytype can be identified. Simpler mica polytypes such as $1M$, $2M_1$, and $2M_2$ can be identified by comparing the films with the standard patterns. All three-layer polytypes and 20 of the 26 four-layer polytypes can also be identified by their cell dimensions, symmetry, and rules for structural extinctions (Ross et al., 1966). Many other polytypes of higher layer repeats, however, can only be identified by comparing their PID functions or S^N functions (Takeda, 1967).

To measure the intensities of complex mica polytypes through the use of a microphotodensitometer, one must obtain well-resolved X-ray diffraction patterns. For preliminary identification, Mo$K\alpha$ radiation is recommended. For mica polytypes with layer numbers $N = 8$–15, Cu$K\alpha$ radiation will give better resolution of the reflections. In the case where $N = 15$–30, Fe$K\alpha$ or preferably Cr$K\alpha$ radiation with a fine slit of diameter 0.3–0.1 mm must be used to obtain well-resolved diffraction patterns.

In practice, it has been found that measurement of the periodic intensity distribution along the following three reciprocal lattice rows is usually sufficient to identify the stacking sequence: $02l$, $11l$, and $\bar{1}1l$. Lattice rows $04l$, $22l$, and $\bar{2}2l$ can be used equally well for identification of the polytype if the reflections are strong enough. Nevertheless, one can observe the PID of a polytype directly on the photograph without any intensity correction and reduction because the Fourier transform of the unit layer of mica is generally constant in the range from 040 to 042 of the $1M$ repeat and also in some other parts of the pattern (see Takeda, 1967, Fig. 2).

For an accurate analysis, the measured intensities must be corrected for L_p factors and absorption. Each F_0 must then be divided by the Fourier transform of the unit layer $G_0(hkl)$ at the location of each reflection. To obtain the values of $G_0(hkl)$, the structure and composition of the

TABLE 3. Types of reciprocal lattice nets for identication of three basic polytypes

Dial reading	Reciprocal lattice plane, $1M$ setting	$1M$	$2M_1$	Reciprocal lattice plane, $2M_2$ setting*	$2M_2$
0**	(0*kl*)	$1M$(0*kl*)	$2M_1$(0*kl*)	(*h*0*l*)	$1M$(*hhl*)
30	(*h*3*hl*)	$1M$(*h*0*l*)†	$1M$(*h*0*l*)†	(3*hhl*)	$2M_2$(0*kl*)
60	(*hhl*)	$1M$(*hhl*)	$2M_1$(*hhl*)	(*hhl*)	$2M_2$(*hhl*)
90	(*h*0*l*)	$1M$(*h*0*l*)	$1M$(*h*0*l*)	(0*kl*)	$2M_2$(0*kl*)*

* Conventional $2M_2$ axial setting of Smith and Yoder (1956). Note that $2M_2$(0*kl*) is the characteristic pattern of $2M_2$.
** Arbitrarily chosen origin.
† In dioctahedral micas, weak spots appear in a reciprocal lattice row with $h = 0$ mod 3.

one-layer mica should be approximately known. If the structure is not known, the method described by Takeda and Sadanaga (1969, Table 1) may be used to evaluate the $G_0(hkl)$.

If the values of S^N are obtained over more than one repeat, the average values should be used to avoid the errors in measurements of F_0 and errors in evaluation of $G_0(hkl)$. Finally, S^N is scaled by making use of the following relation:

$$\sum_{j=1}^{N} [S_j^N(hkl)]^2 = N^2. \quad (4)$$

Analysis of mica stacking sequences

One- and two-layer micas

The method of identifying the six simplest mica polytypes of Smith and Yoder (1956) has been given by previous workers (Zvyagin, 1960; Franzini and Schiaffino, 1963). The major difficulty in identifying the polytypes is mostly due to the complexity of diffraction patterns caused by twinning or by crystals composed of more than one polytype. Smith and Yoder (1956) pointed out the similarity of the single-crystal X-ray diffraction patterns of the twinned $1M$ polytype to those of the $3T$ polytype. A method of analyzing simple twin operations (Sadanaga and Takéuchi, 1961) has been extended by Rieder (1970) in a systematic manner to include complex twins.

Our experience shows that one of the easiest ways for the nonspecialist to identify the simplest mica polytypes is to compare the diffraction patterns with standard patterns such as those given in Table 3. In Table 3 standard patterns for each one- and two-layer mica are shown for a particular dial setting of the precession camera.

Three-layer micas

Two of the six possible three-layer polytypes (Table 4) have interlayer rotations 0 or $\pm 120°$. The two polytypes are called ternary members in this text because their stacking sequence (0, 2, or $\bar{2}$) can be expressed by ternary numbers (0, 1, or 2). Both of them, namely $3T$[222] and $3Tc_1[02\bar{2}]$, are the simplest form of the basic polytype series that commonly occur in nature. The $3T$ polytype is well known because it is one of the six forms described by Smith and Yoder (1956). However, the $3Tc_1$ form is as simple as the $3T$ form and is probably more common than the $6H$ form. The cell dimensions and space group are given by Ross et al. (1966). The other four polytypes, called sixfold (senary) members, can be identified by the axial setting, crystal system, space groups, and any special extra-extinction rules beyond those required for the space group (i.e., structural presence criteria).

Great care should be taken not to identify a complexly twinned crystal as a new polytype. Most of the $3M$ forms reported have been found to be twins. To be sure of the correct stacking sequence, it is recommended that the observed intensities be compared to the calculated characteristic PID as given in Table 4. In spite of their simple stacking sequence, the number of crystals identified as $3T$ appears to be rather small. The intensity distribution displayed by the $3T$ polytype is very similar to that of the $1M$ polytype with $3T$-type twinning, especially in trioctahedral micas. Thus, the intensity distribution should be carefully measured to assure the correctness of a $3T$ stacking sequence. The dioctahedral $3T$[222] mica crystal structures identified to date are: muscovite (Güven and Burnham, 1967; Amisano-Canesi et al., 1994), paragonite (Sidorenko et al., 1977), lepidolite (Brown, 1978), and protolithionite (Pavlishin et al., 1981; Weiss et al., 1993). Sadanaga and Takéuchi (1961) identified a $3T$ trioctahedral polytype by measuring intensity data. No $3T$ polytype was identified by Ross et al. (1966).

Four-layer micas

Among 26 possible four-layer mica polytypes, six polytypes (three ternary and three senary members, Table

TABLE 4. Crystallographic data of all possible three-layer micas

Member*	Stacking sequence	Axial setting	Space group	Calculated PID	
				$S^3(0kL)$**	$S^3(hhL)$ or $S^3(\bar{h}hL)$
Ternary	$3T$[222]	$3T$	$P3_{1,2}12$	1.7, 1.7, 1.7	1.7, 1.7, 1.7
	$3Tc_1[02\bar{2}]$	$3Tc_1(2M_2)$	$C\bar{1}$	1.3, 0.9, 2.5	0.9, 1.3, 2.5
Senary	$3M_1$[033]	$3M_1(2M_1)$	$C2/m$	3.0, 0, 0	1.3, 2.5, 0.9
	$3M_2[11\bar{2}]$	$3M_1$	$C2$	1.7, 1.7, 1.7	0.9, 1.3, 0.9
	$3Tc_2[01\bar{1}]$	$3M_1$	$C\bar{1}$	0, 0, 3.0	0.9, 1.3, 2.5
	$3Tc_3$[123]	$3M_1$	$C1$	1.7, 1.7, 1.7	1.3, 0.9, 2.5

* Ternary polytypes contain no 60, 180, or 300° layer rotations; senary forms contain 60, 180, or 300° layer rotations.
** $L = 0$, 1, and 2.

TABLE 5. Calculated PID functions, $S^4(02L)$, for the four-layer ternary polytypes and related senary polytypes*

RTW symbol	L	$4M_1[020\bar{2}]$	$4M_2[0222]$	$4M_3[2\bar{2}22]$	$4Tc_1[002\bar{2}]$
	0	1.000	2.646	2.000	1.000
	1	1.732	1.732	2.450	0.897
	2	3.000	1.732	0	1.732
	3	1.732	1.732	2.450	3.346
Space group		$C2/c$	$C2$	$C2/c$	$C\bar{1}$
TS symbol		$010\bar{1}$	0010	0011	$011\bar{1}$
Senary counterparts		$4Tc_4[0213]$	$4Tc_3[13\bar{2}\bar{2}]$,** $4Tc_5[0132]$	$4Tc_2[1\bar{1}\bar{2}2]$	$4Tc_{11}[011\bar{2}]$

Note: all polytypes have the $1M$-type axial setting.
* The nine four-layer polytypes that cannot be identified by symmetry and extra-extinctions other than that of space group (see Ross et al., 1966).
** $S^4(11L)$ of $4Tc_3$ has $4Tc_2$-type intensity distribution and thus differs from $4Tc_5$.

5) cannot be identified without comparing their characteristic PID patterns. Three four-layer polytypes have been found in natural and synthetic micas. Another ternary polytype, $4Tc_1[002\bar{2}]$, belongs to the $[0_n2\bar{2}]$ series of mica polytypes that are frequently found, though this particular member of the series has not yet been identified. Other members of senary polytypes are distinguished by the crystallographic data given in Table 6. The extra-extinction rules (Ross et al., 1966), other than those required by the space group, are useful in identifying these simpler mica polytypes, but they are a part of the information contained in the PID function (Takeda, 1967).

The similarities and dissimilarities in intensity distribution between polytypes follow a clear system. Intensities of some reflections (e.g., $00l$) are the same for all mica polytypes within a given sample. Intensities of others (which are called subfamily reflections by adherents to the OD theory) are identical for polytypes within each subfamily. All the ternary polytypes are composed of D layers and give nearly identical $h0l$, $h3hl$, and $\bar{h}3hl$ patterns. This is because the projections of the crystal structure in the direction perpendicular to these three planes are identical. Only the diagnostic reciprocal lattice nets are different and of value in identification. Therefore, the mode of stacking the layers must be defined by examining the $0kl$, hhl, or $\bar{h}hl$ nets, with the crystal structure projections differing in the direction perpendicular to these planes.

TABLE 6. Crystallographic data and $S^4(0kl)$, $S^4(hhl)$, or $S^4(\bar{h}hl)$ for all senary four-layer polytypes

Axial setting	Stacking sequence	Space group	$S^4(0kl)$	$S^4(hhl)$ or $(\bar{h}hl)$
$2O$	$4O_1[0303]$	$Ccmm$	·000	—
	$4O_2[13\bar{1}3]$	$C2cm$	—	—
	$4O_3[23\bar{2}3]$	$Cc2m$	—	·0·0
	$4O_4[1\bar{2}12]$	$C222_1$	—	—
	$4M_6]1\bar{1}\bar{1}1]$	$C2/c$	··0·	—
	$4M_7[01\bar{2}1]$	$C2$	—	—
$1M$	$4M_4[0033]$	$C2/m$	·000	—
	$4M_5[11\bar{2}2]$	$C2$	··0·	—
	$4Tc_2[1\bar{1}\bar{2}2]$	$C\bar{1}$	··0·	·0·0
	$4Tc_3[13\bar{2}\bar{2}]$	$C1$	—	··0·
	$4Tc_4[0213]$	$C1$	—	—
	$4Tc_5[0132]$	$C1$	—	—
	$4Tc_8[2\bar{2}33]$	$C\bar{1}$	·0·0	··0·
	$4Tc_9[1\bar{2}2\bar{1}]$	$C\bar{1}$	—	·0·0
	$4Tc_{10}[001\bar{1}]$	$C\bar{1}$	—	·000
	$4Tc_{11}[011\bar{2}]$	$C1$	—	—
$2M_2$	$4M_8[010\bar{1}]$	$C2/c$	—	·000
	$4M_9[1131]$	$C2$	·0·0	—
	$4M_{10}[12\bar{1}\bar{2}]$	$C2/c$	·0·0	—
	$4M_{11}[1\bar{2}\bar{3}2]$	$C2$	—	··0·
	$4Tc_6[1\bar{1}33]$	$C\bar{1}$	—	··0·
	$4Tc_7[0123]$	$C1$	—	—

Note: the $S(hkl)$ designations for those polytypes that show extra-extinction beyond that required by the space group are as follows: ·000 4.0, 0, 0, 0; ·0·0 2.0, 0, 3.5, 0; ··0· 2.0, 2.4, 0, 2.4. Dash stands for no such extinction.

Of the 26 possible four-layer mica polytypes, nine cannot be distinguished by symmetry and structural presence criteria alone (Ross et al., 1966). These nine polytypes are listed in Table 5 and include four ternary and five senary forms. Symmetry and a use of the PID function, as expressed along the $02L$ reciprocal lattice row line, $S^4(02L)$, distinguish seven of the nine polytypes. The other two polytypes ($4Tc_3$, $4Tc_5$) can be distinguished by examining both the $02L$ and $11L$ row lines and comparing these to the $S^4(02L)$ and $S^4(11L)$ calculated PID functions.

Three polytypes in Table 5 have been identified. The $4M_2[0222]$ form has been reported by Ross et al. (1966) and $4Tc_5[0132]$ by Takeda (1967). The $4M_1[020\bar{2}]$polytype has been found in synthetic fluorphlogopite coexisting with $1M$ mica (T. Nishida, 1969 personal communication).

For those polytypes with layer number larger than four, the method of identification, on the basis of symmetry and visual inspection, used for the four layer polytypes is not always efficient. To identify the more complex mica polytype, the PID functions along several reciprocal lattice rows and symmetry elements must be generated for all possible N-layer polytypes. These data (Tables 7–10) are then compared to the observed diffraction data to define the particular stacking sequence.

RESULTS

The most common polytypes among complex stacking sequences are based on the $1M$ form with a single 120° periodic stacking fault introduced every n layers (Ross et al., 1966). The series is represented by the symbol $[(0)_n2\bar{2}]$. The PID functions of the polytypes belonging to this series have special characteristics: a strong peak at every Nth reflection (where $N = n + 2$) along an $0kl$ row line and a rapid decrease of intensity in an asymmetrical way from each strong Nth reflection (see Fig. 1 of Ross et al., 1966).

TABLE 7. The PID functions, $S^N(02L)$, of mica polytypes belonging to the $1M$ series

Polytype symbol	Axial setting	L = 0 / 12	1 / 13	2 / 14	3 / 15	4 / 16	5 / 17	6 / 18	7 / 19	8 / 20	9 / 21	10 / 22	11 / 23
$5Tc_1$	$1M$	1.00	2.13	4.17	1.17	0.87							
$6Tc_1$	$3Tc_1$	1.35	0.92	0.88	1.13	2.53	4.99						
$7Tc_1$	$1M$	1.00	0.87	0.93	1.27	2.94	5.81	1.54					
$8Tc_1$	$1M$	1.00	1.42	3.35	6.63	1.73	1.09	0.90	0.87				
$9Tc_1$	$9Tc_1$	3.76	1.58	1.08	0.90	0.87	0.94	1.19	1.93	7.46			
$10Tc_1$	$1M$	1.00	0.89	0.87	0.95	1.17	1.73	4.17	8.29	2.13	1.29		
$11Tc_1$	$1M$	1.00	1.26	1.89	4.58	9.11	2.33	1.40	1.06	0.92	0.87	0.89	
$12Tc_1$	$3Tc_1$	1.35	1.06	0.92	0.87	0.88	0.96	1.13	1.51	2.53	9.94	4.99	2.05
$13Tc_1$	$1M$	1.00 1.20	0.90	0.87	0.88	0.96	1.12	1.44	2.21	5.40	10.76	2.73	1.62
$14Tc_1$	$1M$	1.00 0.87	1.18 0.91	1.54	2.37	5.81	11.59	2.94	1.73	1.27	1.05	0.93	0.88
$15Tc_1$	$3Tc_1$	1.35 12.42	1.10 3.14	0.96 1.84	0.89	0.87	0.88	0.93	1.04	1.25	1.63	2.53	6.22
$16Tc_1$	$1M$	1.00 3.35	0.91 1.96	0.87 1.42	0.87 1.15	0.90	0.97	1.09	1.31	1.73	2.69	6.63	13.24
$17Tc_1$	$1M$	1.00 0.94	1.14 0.89	1.38 0.87	1.83 0.88	2.86 0.92	7.05	14.07	3.55	2.07	1.50	1.21	1.04
$18Tc_1$	$9Tc_1$	3.76 1.19	2.19 1.45	1.58 1.93	1.26 3.02	1.08 7.46	0.97 14.89	0.90	0.87	0.87	0.89	0.94	1.04
$19Tc_1$	$1M$	1.00 7.87	0.92 15.72	0.88 3.96	0.87 2.30	0.87 1.65	0.91 1.32	0.97 1.12	1.07	1.24	1.52	2.03	3.18
$20Tc_1$	$1M$	1.00 1.17	1.11 1.03	1.29 0.95	1.59 0.90	2.13 0.87	3.35 0.87	8.29 0.89	16.55 0.93	4.17	2.42	1.73	1.38
$21Tc_1$	$3Tc_1$	1.35 1.43	1.16 1.81	1.03 2.53	0.95 4.37	0.90 17.37	0.87 8.70	0.87 3.51	0.88 2.23	0.91 1.66	0.97	1.07	1.21
$22Tc_1$	$1M$	1.00 2.33	0.93 3.67	0.89 9.11	0.87 18.20	0.87 4.58	0.88 2.65	0.92 1.89	0.97 1.49	1.06 1.26	1.20 1.10	1.40	1.73
$23Tc_1$	$1M$	1.00 1.55	1.10 1.30	1.24 1.14	1.46 1.03	1.80 0.95	2.43 0.91	3.84 0.88	9.52 0.87	19.03 0.87	4.78 0.89	2.76 0.94	1.97

The PID functions of this series with $N = 5$–23 are given in Table 7. Their axial settings indicate the position $L = 0$ and are in accordance with the convention of Takeda and Sadanaga (1969). Within this series Ross et al. (1966) reported the following: $3Tc_1(02\bar{2})$, $8Tc_1[(0)_6 2\bar{2}]$, $14Tc_1[(0)_{12}2\bar{2}]$, and $23Tc_1[(0)_{21}2\bar{2}]$. The $3Tc_1$ form, already described above, is the simplest of the series. Among the four-layer micas $4Tc_1[002\bar{2}]$ is most likely to be found, but Zvyagin (1960) predicted that $4M_3[2\bar{2}\bar{2}2]$ should also occur because of its high symmetry. Rieder (1970) identified the $9Tc_1[(0)_7 2\bar{2}]$ in Li- and Fe-bearing micas from the Krusné Mountains (Erzgebirge). The $8Tc_{12}[00022\bar{2}02]$ polytype (Table 8) has a more complex sequence (Ross et al., 1966, Fig. 1) but has also been interpreted as a modification of the $1M$ basic series.

Another common series is based on the $3T$ basic polytype. General symbols are given as $[(222)_n 0]$ for the $(3n + 1)$ layer polytypes and $[(222)_n 2\bar{2}]$ for the $(3n + 2)$ layer ones. Examples found in nature include $4M_2(0222)$, $8M_8[(222)_2 2\bar{2}]$, and $11M_1[(222)_3 2\bar{2}]$. The PID functions of the $3T$ series are given in Table 9.

The $10Tc_3[0022222\bar{2}22]$ polytype is also considered to

TABLE 8. Examples of the PID functions $S^8(02L)$ for some eight-layer polytypes with modified $1M$ series related to $8Tc_{12}$

Polytype symbol	Axial setting	L = 0	1	2	3	4	5	6	7
$8Tc_{12}$	$1M$	2.000	1.326	1.268	3.200	3.464	3.200	4.732	1.326
$8M_2$	$1M$	6.557	1.732	1.732	1.732	1.732	1.732	1.732	1.732
$8Tc_4$	$1M$	1.000	2.039	2.608	2.548	1.732	4.923	4.147	1.055
$8M_9$	$1M$	5.292	3.200	2.450	1.326	0.000	1.326	2.450	3.200
$8M_{14}$	$1M$	5.292	2.450	0.000	2.450	3.464	2.450	0.000	2.450
$8Tc_2$	$1M$	2.000	1.614	1.268	0.836	0.000	5.078	4.732	2.628
$8Tc_{36}$	$1M$	2.000	3.887	0.000	4.857	3.464	2.982	0.000	0.639

Note: stacking sequences: $8Tc_{12}[00022\bar{2}02]$, $8M_2[00000222]$, $8Tc_4[00002202]$, $8M_9[00002\bar{2}\bar{2}2]$, $8M_{14}[00022\bar{2}22]$, $8Tc_2[0000020\bar{2}]$, $8Tc_{36}[002\bar{2}2\bar{2}2\bar{2}]$.

TABLE 9. The PID functions, $S^N(02L)$, of the $3T$-series polytypes

Polytype symbol	L											
	0	1	2	3	4	5	6	7	8	9	10	11
$5M_3$	2.65	1.07	2.80	2.80	1.07							
$7M_3$	4.36	0.77	3.12	2.16								
$8M_3$	4.36	0.72	1.73	4.18	1.73							
$10M_3$	6.08	0.66	1.07	4.53	2.80	1.73						
$11M_3$	6.08	0.65	0.95	2.42	5.59	1.88	1.88					
$13M_3$	7.81	0.63	0.81	1.40	5.96	3.48	1.84					
$14M_3$	7.81	0.62	0.77	1.20	3.12	7.01	2.16	1.73				
$16M_3$	9.54	0.61	0.72	0.98	1.73	7.38	4.18	2.04	1.73			
$17M_3$	9.54	0.60	0.70	0.92	1.46	3.83	8.44	2.47	1.79			
$19M_3$	11.27	0.60	0.67	0.83	1.16	2.07	8.81	4.89	2.28	1.78		
$20M_3$	11.27	0.60	0.66	0.80	1.07	1.73	4.53	9.87	2.80	1.92	1.73	
$22M_3$	13.00	0.59	0.65	0.75	0.95	1.35	2.42	10.24	5.59	2.54	1.88	1.73

Note: stacking sequences with layer numbers $N = 3n$ (n is an integer) do not yield the $3T$ series. Polytype $8M_3 = 8M_8$ of Ross et al. (1966), and $11M_3 = 11M_1$ of Ross et al. (1966).

be a modification of the $3T$ basic series. This polytype reveals the same PID intensities as those of the monoclinic ones, but the stacking sequence reveals triclinic symmetry. Theoretical studies of this mica polytype are given by Sadanaga and Takeda (1968), who proposed diffraction enhancement of symmetry from triclinic to monoclinic.

Mica polytypes related to the $2M_1$ basic polytype are expected because the $2M_1$ polytype is commonly found in nature (Güven, 1971). A $24Tc$ biotite has been reported by Hendricks and Jefferson (1939) from Ambulawa, Ceylon. Smith and Yoder (1956) mentioned that this $24Tc$ biotite is a twin of the $8Tc$ polytype, but they did not determine the stacking sequence. Takeda (1969) derived PID values from the intensity distribution given in the literature for this $24Tc$ biotite. The calculated PID functions for various eight-layer polytypes (Table 10) shows that the $24Tc$ mica is a twinned $8Tc_2[(2\bar{2})_3\bar{2}2]$ polytype (Fig. 1).

DISCUSSION

Of the six predicted ordered mica polytypes (Smith and Yoder, 1956), only the $6H$ polytype has not yet been found in nature. The rarity or nonoccurrence of the $2O$, $2M_2$, and $6H$ mica polytypes is explained by the ditrigonal nature of most mica unit layers. The trigonal arrangement of the basal O atoms prevents stacking of the unit layers by other than 0 or $\pm 120°$ rotations. Thus, the $6H$, $2O$, and $2M_2$ polytypes, which require 60 or 180° rotations, are very rare (Rule et al., 1987).

The stacking sequences of complex mica polytypes determined by application of the PID function (Ross et al., 1966; Takeda, 1967) have revealed that mica polytypes with smaller layer numbers than $6H$ occur quite frequently. Many of the mica polytypes thus far identified have layer stacking sequences based on the $1M$ or the $3T$ polytypes and form the $1M$ and $3T$ series. In addition to the $1M$ and $3T$ series, we propose that $2M_1$ is a basic structure because $8Tc_2$ (former $24Tc$ of Hendricks and Jefferson, 1939) is based on the $2M_1$ sequence with a periodic stacking fault.

Basic structures found in the mica polytypes, such as the $1M$, $2M_1$, and $3T$ series, are also found in silicon carbide. The basic series found in silicon carbide are suggested to be caused by spiral growth (Frank, 1951). The presence of these series in mica suggests that the mechanism of generating the complex mica polytypes may also be explained by spiral growth. This origin for mica polytypism has been examined by Baronnet (1975) in his study of growth spirals in complex mica polytypes. Supported by their observations on synthetic as well as natural micas, Baronnet and Kang (1989) proposed that the principles of the perfect-matrix (Baronnet, 1975) and faulted-matrix (Baronnet et al., 1981) models of screw dislocation theory of polytypism can explain the origin of most of the complex polytypes of micas.

TABLE 10. The PID functions, $S^N(02L)$, of mica polytypes of the $2M_1$ series

Polytype symbol	Axial setting	L											
		0	1	2	3	4	5	6	7	8	9	10	11
$5Tc_2$	$1M$	1.00	1.17	2.13	0.87	4.17							
$6Tc_2$	$3Tc_1$	3.88	0.60	0.47	3.26	1.65	2.65						
$7Tc_2$	$1M$	1.00	5.81	1.27	0.87	1.54	2.94	0.93					
$8Tc_2$	$1M$	1.00	0.23	0.90	4.07	1.73	1.78	3.35	5.31				
$9Tc_2$	$9Tc_1$	0.87	1.08	3.76	1.93	0.94	0.90	1.58	7.46	1.19			
$10Tc_2$	$1M$	2.00	4.05	6.74	1.37	0.54	0.00	1.32	4.90	1.89	1.66		
$11Tc_2$	$1M$	1.00	0.87	1.06	2.33	4.58	1.26	0.89	0.92	1.40	9.11	1.89	
$12Tc_2$	$3Tc_1$	2.06	5.72	1.73	0.20	0.31	0.78	1.73	8.17	4.76	2.25	1.73	1.67

Note: stacking sequences are $[(2\bar{2})_n\bar{2}2]$ or $[(2\bar{2})_n0]$.

On the basis of the structural refinements of coexisting $1M$ and $2M_1$ polytypes, Takeda and Ross (1975) proposed that the structure of a particular unit layer of a polytype is directly related to the atomic and geometric constraints imposed upon it by the two adjacent unit layers, the constraints varying with the relative orientation of the OH bond in the adjacent layers. Thus, the unit layer of the $1M$ polytype with adjacent layers in 0° relative orientation has a crystal structure slightly different from that of the unit layer of the $2M_1$ polytype, which has adjacent layers in $\pm 120°$ relative orientation. It is further proposed that once interlayer constraints form between adjacent layers, these constraints tend to control the orientation of the next nucleated layer so as to give an ordered stacking sequence, usually of the $1M$ or $2M_1$ type and, more rarely, the $3T$ type. Once a sequence of layers has formed through layer-by-layer nucleation, further crystal growth often occurs by means of a spiral growth mechanism. The polytypic form of the final crystal is controlled by the sequence of layers within the primary platelet and within the dislocation step.

Graphic examination of the complex stacking sequences (Fig. 1), which are not readily explained by the faulted-matrix model (Baronnet and Kang, 1989), suggests the following general observation (Baronnet and Takeda, unpublished data). When a stacking fault is introduced within one of the $1M$, $3T$, and $2M_1$ structures, the next layer or the next few layers are so stacked that the last stacking vectors return as closely as possible to the direction parallel to the original direction of the basic stacking sequences (Fig. 1), and these layers form a new unit for subsequent growth. This has been confirmed by a recent HRTEM study of stacking faults in a biotite single crystal (Baronnet et al., 1992).

We present the following hypothesis, which should be tested in future studies. When a stacking fault is generated in the basic polytype structure, the orientation of the next layer to be stacked on top of the faulted one will be influenced by the stacking sequences of the previous layers, and, within the next one or several steps, the orientation of the stacking direction will be recovered as closely as possible to the original direction. Further crystal growth then occurs by means of a spiral growth mechanism to retain the stacking order.

This recovery process of the faulted matrix may be controlled by a statistical process similar to a "random walk" and constrained for only a few short steps. Therefore it cannot be rigorously predicted because the influence of the preceding stacking sequence may not be strong. The mode of the stacking sequences found in a clintonite "valuevite" crystal (Ohta et al., 1978) shows such a statistical process. Another mechanism for the above recovering sequence was proposed by Takeda and Ross (1993). During spiral growth of a basic polytype, a platelet with a stacking fault deposited on a part of the spiral surface may retain the same orientation as that of the basic sequence if the spiral grows over the platelet and covers it in such a manner that the bottom of the covering layer shifts laterally to match the sequence of the top of the platelet. Further studies are required to determine some of the more complex mica polytypes by the method described in this paper.

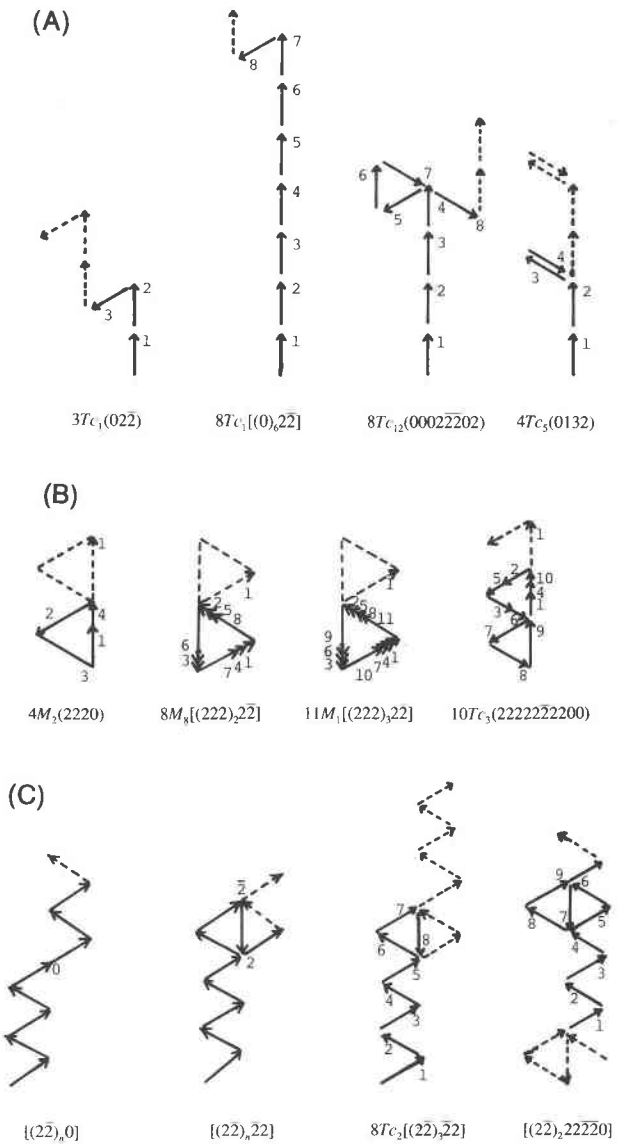

Fig. 1. Examples of stacking sequences of observed complex mica polytypes represented by their stacking vectors (Ross et al., 1966). (**A**) $1M$ series, (**B**) $3T$ series, and (**C**) $2M_1$ series.

ACKNOWLEDGMENTS

We thank R. Sadanaga, emeritus professor, University of Tokyo, and Alain Baronnet, Centre de recherche sur les mechanismes de la croissance cristalline (CRMC²), Marseille, France, and the late D.R. Wones, Virginia Polytechnic Institute and State University, for their valuable advice. The computations were performed on a HITAC 8800/8700 computer at the Computer Center of University of Tokyo. Work on this paper was continued while one of the authors (H.T.) was a JSPS/CNRS fellow at CRMC² in the fall of 1990 and a JSPS/CNR fellow at University of Padua, Italy, in 1994. We thank Alain Baronnet, CRMC², and D.R. Veblen, Johns Hopkins University, for critical reading of the manuscript, and K. Hash-

imoto for typing this manuscript. A part of this work was supported by a Scientific Grant of the Ministry of Education, Science and Culture, and by the Tokyo Club.

References cited

Amelinckx, S., and Dekeyser, W. (1953) Le polytypisme des minéraux micacés et argileux. Premiere partie: Observation et leurs interprétations. Comptes Rendus XIX International Geological Congress, 18, 9–22.

Amisano-Canesi, A., Chiari, G., Ferraris, G., Ivaldi, G., and Soboleva, S.V. (1994) Muscovite- and phengite-3*T*: Crystal structure and conditions of formation. European Journal of Mineralogy, 6, 489–496.

Baronnet, A. (1975) Growth spirals and complex polytypism in micas: I. Polytypic structure generation. Acta Crystallographica, A31, 345–355.

Baronnet, A., and Kang, Z.C. (1989) About the origin of mica polytypes. Phase Transitions, 16/17, 477–493.

Baronnet, A., Pandey, D., and Krishna, P. (1981) Application of the faulted matrix model to the growth of polytype structures in mica. Journal of Crystal Growth, 52, 963–968.

Baronnet, A., Nitsche, S., and Kang, Z.C. (1992) Layer stacking microstructures in a biotite single crystal. Phase Transitions, 43, 107–128.

Brown, B.E. (1978) The crystal structure of a 3*T* lepidolite. American Mineralogist, 63, 332–336.

Burnham, C.W., and Radoslovich, E.W. (1964) Crystal structures of coexisting muscovite and paragonite. Carnegie Institution of Washington Year Book, 63, 232–236.

Dornberger-Schiff, K., Backhaus, K.-O., and Durovic, S. (1982) Polytypism of micas: OD-interpretation, stacking symbols, symmetry relations. Clays and Clay Minerals, 30, 364–374.

Frank, F.C. (1951) The growth of carborundum: Dislocations and polytypism. Philosophical Magazine, 42, 1014–1421.

Franzini, M., and Schiaffino, L. (1963) On the crystal structure of biotites. Zeitschrift für Kristallographie, 119, 297–309.

Guinier, A. (1963) X-ray diffraction in crystals, imperfect crystals, and amorphous bodies. 378 p. Freeman, San Francisco, California.

Guinier, A., et al. (1984) Nomenclature of polytype structures: Report of the International Union of Crystallography Ad-Hoc Committee on the nomenclature of disordered, modulated and polytype structures. Acta Crystallographica, A40, 399–404.

Güven, N. (1971) Structural factors controlling stacking sequences in dioctahedral micas. Clays and Clay Minerals, 19, 159–165.

Güven, N., and Burnham, C.W. (1967) The crystal structure of 3*T* muscovite. Zeitschrift für Kristallographie, 125, 163–183.

Hendricks, S.B., and Jefferson, M.E. (1939) Polymorphism of the micas with optical measurements. American Mineralogist, 24, 729–771.

Lipson, H., and Taylor, C.A. (1958) Fourier transforms and X-ray diffraction. 76 p. Bell, London.

Mogami, K., Nomura, K., Miyamoto, M., Takeda, H., and Sadanaga, R. (1978) On the number of distinct polytypes of mica and SiC with a prime layer-number. Canadian Mineralogist, 16, 427–435.

Ohta, T., Takéuchi, Y., and Takeda, H. (1978) Structural study of brittle micas (II): Statistical mode of stacking sequence in a valuevite crystal as deduced by computer simulation. Mineralogical Journal, 9, 1–15.

Pandey, D., Baronnet, A., and Krishna, P. (1982) Influence of stacking faults in the growth of polytype structures in mica. Physics and Chemistry of Minerals, 8, 268–278.

Pavlishin, V.I., Semenova, T.F., and Rozhdestvenskaya, I.V. (1981) Protolithionite-3*T*: Its structure, typomorphism, and practical significance. Mineralogicheskii Zhurnal, 1, 47–60.

Rieder, M. (1970) Lithium-iron micas from the Krusné Hory Mountains (Erzgebirge): Twins, epitactic overgrowths and polytypes. Zeitschrift für Kristallographie, 132, 161–184.

Ross, M., Takeda, H., and Wones, D.R. (1966) Mica polytypes: Systematic description and identification. Science, 151, 191–193.

Rule, A.C., Bailey, S.W., Livi, K.J.T., and Veblen, D.R. (1987) Complex stacking sequences in a lepidolite from Tørdal, Norway. American Mineralogist, 72, 1163–1169.

Sadanaga, R., and Takeda, H. (1968) Monoclinic diffraction patterns produced by certain triclinic crystals and diffraction enhancement of symmetry. Acta Crystallographica, B24, 144–149.

Sadanaga, R., and Takéuchi, Y. (1961) Polysynthetic twinning of micas. Zeitschrift für Kristallographie, 116, 406–429.

Sidorenko, O.V., Zvyagin, B.B., and Soboleva, S.V. (1977) The crystal structure of 3*T* paragonite. Kristallografiya, 22, 976–981.

Smith, J.V., and Yoder, H.S. (1956) Experimental and theoretical studies of the mica polymorphs. Mineralogical Magazine, 31, 209–235.

Takeda, H. (1967) Determination of the layer stacking sequence of a new complex mica polytype: A 4-layer lithium fluorophlogopite. Acta Crystallographica, 22, 845–853.

——— (1969) Existence of complex mica polytype series based on $2M_1$ sequence, p. 2–3. Abstract Autumn Meeting of Mineralogical Society, Iwate, Japan.

——— (1971) Distribution of mica polytypes among space groups. American Mineralogist, 56, 1042–1056.

Takeda, H., and Morosin, B. (1975) Comparison of observed and predicted structural parameters of mica at high temperature. Acta Crystallographica, B31, 2444–2452.

Takeda, H., and Ross, M. (1975) Mica polytypism: Dissimilarities in the crystal structures of coexisting 1*M* and $2M_1$ biotite. American Mineralogist, 60, 1030–1040.

——— (1993) Most common mica polytypes and their formation mechanism, p. 113. Abstract Annual Meeting Crystallographic Society of Japan, Tokyo, Japan.

Takeda, H., and Sadanaga, R. (1969) New unit layers for micas. Mineralogical Journal, 5, 434–449.

Weiss, Z., and Wiewiora, A. (1986) Polytypism of micas: III. X-ray diffraction identification. Clays and Clay Minerals, 34, 53–68.

Weiss, Z., Rieder, M., Smrcok, L., Petricek, V., and Bailey, S.W. (1993) Refinement of the crystal structures of two "protolithionites." European Journal of Mineralogy, 5, 493–502.

Wood, E.A. (1964) The 80 diperiodic groups in three dimensions. Bell System Technical Journal, 43, 541–559.

Zvyagin, B.B. (1960) Theory of mica polymorphism. Kristallografiya, 6, 714.

Manuscript received September 2, 1994
Manuscript accepted March 13, 1995